between two CH_3 groups, which assumes the interaction can be treated with a Lennard-Jones potential (*27*).

24. J. H. Hoh, J. P. Cleveland, C. B. Prater, J.-P. Revel, P. K. Hansma, *J. Am. Chem. Soc.* **114**, 4917 (1992).
25. G. Liu and M. B. Salmeron, *Langmuir* **10**, 367 (1994).
26. It has been suggested on the basis of SFA studies of different hydrocarbon-terminated layers that it is the hysteresis in adhesion that will correlate with friction (*3*). We believe that in comparisons of chemically distinct functional groups, which exhibit large differences in adhesive interaction, friction differences are directly related to the variations in the adhesive forces.
27. A. Noy, C. D. Frisbie, C. M. Lieber, unpublished results.
28. E. W. Wollman, D. Kang, C. D. Frisbie, I. M. Lorkovic, M. S. Wrighton, *J. Am. Chem. Soc.* **116**, 4395 (1994); L. F. Rozsnyai and M. S. Wrighton, unpublished results.
29. G. P. López, H. A. Biebuyck, C. D. Frisbie, G. M. Whitesides, *Science* **260**, 647 (1993).

30. The spherical tungsten particles used as end-masses were provided by J. P. Cleveland. C.M.L. acknowledges support by the Office of Naval Research and Air Force Office of Scientific Research. C.D.F. acknowledges the National Science Foundation (NSF) for a postdoctoral fellowship (CHE-9302409), and M.S.W. also thanks the NSF for financial support.

30 June 1994; accepted 12 August 1994

Superconductivity in $SrCuO_2$-$BaCuO_2$ Superlattices: Formation of Artificially Layered Superconducting Materials

D. P. Norton, B. C. Chakoumakos, J. D. Budai, D. H. Lowndes, B. C. Sales, J. R. Thompson, D. K. Christen

Pulsed-laser deposition was used to synthesize artificially layered high-temperature superconductors. Thin-film compounds were formed when the constraint of epitaxy was used to stabilize $SrCuO_2$-$BaCuO_2$ superlattices in the infinite layer structure. Using this approach, two new structural families, $Ba_2Sr_{n-1}Cu_{n+1}O_{2n+2+\delta}$ and $Ba_4Sr_{n-1}Cu_{n+3}O_{2n+6+\delta}$, have been synthesized; these families superconduct at temperatures as high as 70 kelvin.

Since the discovery of high-temperature superconductivity (HTSc) (*1*), intensive efforts have revealed numerous families of layered crystal structures containing copper oxide layers (*2*), with superconducting transition temperatures (T_c) as high as 135 K for the Hg-containing cuprates (*3*). Typically, bulk synthesis techniques have been the primary tool in the search for new HTSc materials. Recently, high-pressure synthesis methods have been used to make metastable cuprate phases (*4–7*). However, thin-film growth methods offer unique advantages for the atomic engineering of new HTSc materials because with this technique it is possible to form artificially layered crystal structures. Moreover, the surfaces of single-crystal substrates provide an atomic template that can be used to stabilize epitaxial films in metastable crystal structures.

Advances in the understanding of epitaxial thin-film growth of the cuprates have heightened interest in the possibility of creating artificially layered materials (*8–10*). The cuprate superconductors are ideal candidates for study because their crystal structures are composed of chemically distinct layer modules, the most important of which is the square CuO_2 layer. A prelude to this development has been the epitaxial stabilization of "infinite layer" $(Ca,Sr)CuO_2$ single-crystal thin films (*11–14*). The infinite layer $(Ca,Sr)CuO_2$ structure type, consisting of square CuO_2 layers alternately stacked with square layers of alkaline-earth atoms, is the simplest cuprate with the essential structural features for HTSc (*15*). Indeed, the infinite layer structure can be viewed as a fundamental building unit of all of the HTSc cuprates. Already, by the addition of infinite layer $(Ca,Sr)CuO_2$ modules, metastable thin-film structures of $Bi_2Sr_2Ca_{n-1}Cu_nO_{2n+4}$ have been extended to $n > 3$ with the use of molecular beam epitaxy (MBE) and laser-MBE growth techniques (*16, 17*). In recent pioneering work, laser-MBE, in conjunction with reflection high-energy electron diffraction to monitor the film growth process, was used to grow the first artificially layered HTSc films, which were tentatively identified as 3 unit cells–1 unit cell $BaCuO_2$-$CaCuO_2$ infinite layer superlattices (*18*).

We report here the synthesis of two series of artificially layered HTSc compounds, grown as $SrCuO_2$-$BaCuO_2$ crystalline superlattice structures. Although earlier efforts to grow artificially layered cuprate structures have been restricted to sophisticated MBE-like apparatus with in situ surface analysis techniques (*8, 16–18*), we have formed these materials using only pulsed-laser deposition (PLD). By sequentially depositing from $BaCuO_2$ and $SrCuO_2$ ablation targets in a PLD system, we constructed artificially layered crystalline materials in which the layering sequence was controlled on nearly the atomic-layer scale. The $SrCuO_2$ and $BaCuO_2$ layers are epitaxially stabilized in the infinite layer structure and form the building blocks for the compounds. In the infinite layer structure, $SrCuO_2$ is an insulator, whereas $BaCuO_2$ normally does not form the infinite layer structure, even when high-pressure synthesis techniques are used.

Using this approach, we synthesized two new HTSc series, $Ba_2Sr_{n-1}Cu_{n+1}O_{2n+2+\delta}$ and $Ba_4Sr_{n-1}Cu_{n+3}O_{2n+6+\delta}$, with T_c(onset) as high as 70 K and T_c(resistance R = 0) as high as 50 K.

The $Ba_2Sr_{n-1}Cu_{n+1}O_{2n+2+\delta}$ series, with n = 2, 3, and 4, is structurally analogous to the recently discovered $CuBa_2Ca_{n-1}Cu_nO_{2n+2+\delta}$ high-pressure HTSc phase (*4–6*) and is obtained by artificially layering two unit cells of $BaCuO_2$ and (n − 1) unit cells of $SrCuO_2$ in the infinite layer crystal structure. A schematic of the n = 3 member is shown in Fig. 1. The $Ba_4Sr_{n-1}Cu_{n+3}O_{2n+6+\delta}$ series, formed by layering four unit cells of $BaCuO_2$ and (n − 1) unit cells of $SrCuO_2$ in the infinite layer structure, exhibits superconductivity for the n = 3 member with T_c(onset) = 70 K and T_c(R = 0) = 40 K. In addition, we have epitaxially stabilized 4.0-nm-thick layers of the n = 1 member, infinite layer $BaCuO_2$, in $SrCuO_2$-$BaCuO_2$ multilayer structures that show metallic conductivity and superconductivity at T_c(onset) ≈ 70 K.

We prepared the films on (100) $SrTiO_3$

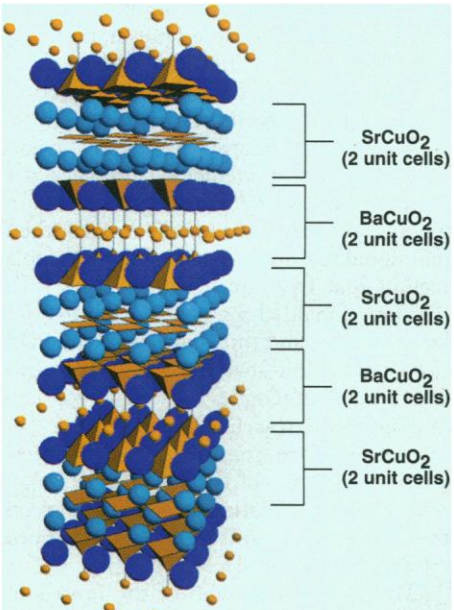

Fig. 1. Structural model of a 2 × 2 $SrCuO_2$-$BaCuO_2$ superlattice compound, also designated as $Ba_2Sr_2Cu_4O_{8+\delta}$. The Ba, Sr, and Cu atoms are represented by the large, medium, and small spheres, respectively. The CuO_4 and CuO_5 units are shown as shaded polyhedra.

Solid State Division, Oak Ridge National Laboratory, Post Office Box 2008, Oak Ridge, TN 37831-6056, USA.

substrates, using conventional multitarget PLD (*11*). Polycrystalline, orthorhombic $SrCuO_2$ and cubic $BaCuO_2$ ablation targets were mounted in a multitarget carousel. The $SrCuO_2$ target was made by solid-state reaction of a mixture of high-purity $SrCO_3$ and CuO, which was pressed and fired at 1025°C. Powder x-ray diffraction confirmed complete decomposition of the carbonates. We prepared the $BaCuO_2$ target using high-purity $BaCuO_2$ powder. The (100) $SrTiO_3$ substrates were cleaned with solvents before being mounted with silver paint on the substrate heater. The ablation beam of the KrF excimer laser was focused to a 1-cm horizontal line and vertically scanned over the targets to improve the uniformity of the film thickness. The focused energy density of the laser was approximately 2 J/cm^2, and the substrates, heated to 600°C, were placed 10 cm from the ablation targets. Film growth was carried out in an oxygen pressure of 200 mtorr.

Before growing the layered structures, a 9.0-nm-thick $SrCuO_2$ buffer layer was grown to initiate epitaxial growth of the infinite layer structure. The average film growth rates were 0.3 Å/s for $SrCuO_2$ and 0.43 Å/s for $BaCuO_2$ in the infinite layer structure. The $Ba_2Sr_{n-1}Cu_{n+1}O_{2n+2+\delta}$ and $Ba_4Sr_{n-1}Cu_{n+3}O_{2n+6+\delta}$ films were grown by alternate ablation from $SrCuO_2$ and $BaCuO_2$ targets for a predetermined number of laser pulses. We controlled the $SrCuO_2$ and $BaCuO_2$ layer thicknesses by counting laser pulses, with the growth rate per laser pulse calibrated from thickness measurements of $SrCuO_2$ films and from the subsequent x-ray diffraction patterns of $SrCuO_2$-$BaCuO_2$ superlattice structures. The total film thickness varied from 90 to 120 nm, corresponding to 60 or more unit cells of $Ba_2Sr_{n-1}Cu_{n+1}O_{2n+2+\delta}$ or $Ba_4Sr_{n-1}Cu_{n+3}O_{2n+6+\delta}$. After deposition, the films were cooled at ~80°C/min in an oxygen pressure of 200 mtorr, with the pressure increased to 760 torr at 375°C.

These materials, fabricated by alternate ablation of $SrCuO_2$ and $BaCuO_2$ targets, can be nominally described either as $Ba_2Sr_{n-1}Cu_{n+1}O_{2n+2+\delta}$ and $Ba_4Sr_{n-1}Cu_{n+3}O_{2n+6+\delta}$, or as $M \times N$ $SrCuO_2$-$BaCuO_2$ superlattices, where M and N are the number of infinite-layer $SrCuO_2$ and $BaCuO_2$ unit cells, respectively, per superlattice period, with $N = 2$ for $Ba_2Sr_{n-1}Cu_{n+1}O_{2n+2+\delta}$ and $N = 4$ for $Ba_4Sr_{n-1}Cu_{n+3}O_{2n+6+\delta}$. The formation of any particular artificially layered phase depends on the precision with which growth of the constituent $BaCuO_2$ and $SrCuO_2$ layers can be controlled. X-ray diffraction patterns give a direct measure of the accuracy of the artificially layered growth scheme in producing the intended structure.

The x-ray diffraction patterns for the $Ba_2Sr_{n-1}Cu_{n+1}O_{2n+2+\delta}$ films with $n = 4$, 3, and 2 (Fig. 2) indicate the presence of multilayer modulation along the *c* axis. Although the diffraction peaks are close to the ideal (00ℓ) locations, some of the peak intensities are weaker than that predicted from structure calculations, with slight deviations or splitting of some of the peaks about the expected peak locations. The most consistent interpretation of these diffraction patterns is to view the peaks as originating either from the structural modulation or from the superlattice chemical modulation. The structural modulation arises from the crystallinity of the compound. It represents, for instance, the average cation spacing along the *c* axis (the growth direction), with some structure peaks present even with no Ba-Sr chemical modulation. For instance, the (003) and (006) peaks for $Ba_2SrCu_3O_{6+\delta}$ would be present for an infinite layer alloy film with no Ba-Sr ordering along the *c* axis. Only as Ba-Sr ordering is realized are other (00ℓ) structure peaks expected. If the Ba-Sr chemical modulation is slightly incommensurate with the structural modulation, superlattice satellite peaks will be present on either side of strong structural peaks at positions that deviate from the ideal (00ℓ) locations.

Peaks from the structural and chemical periodicities converge if the deposition process yields exactly integral numbers of $SrCuO_2$ and $BaCuO_2$ infinite layer unit

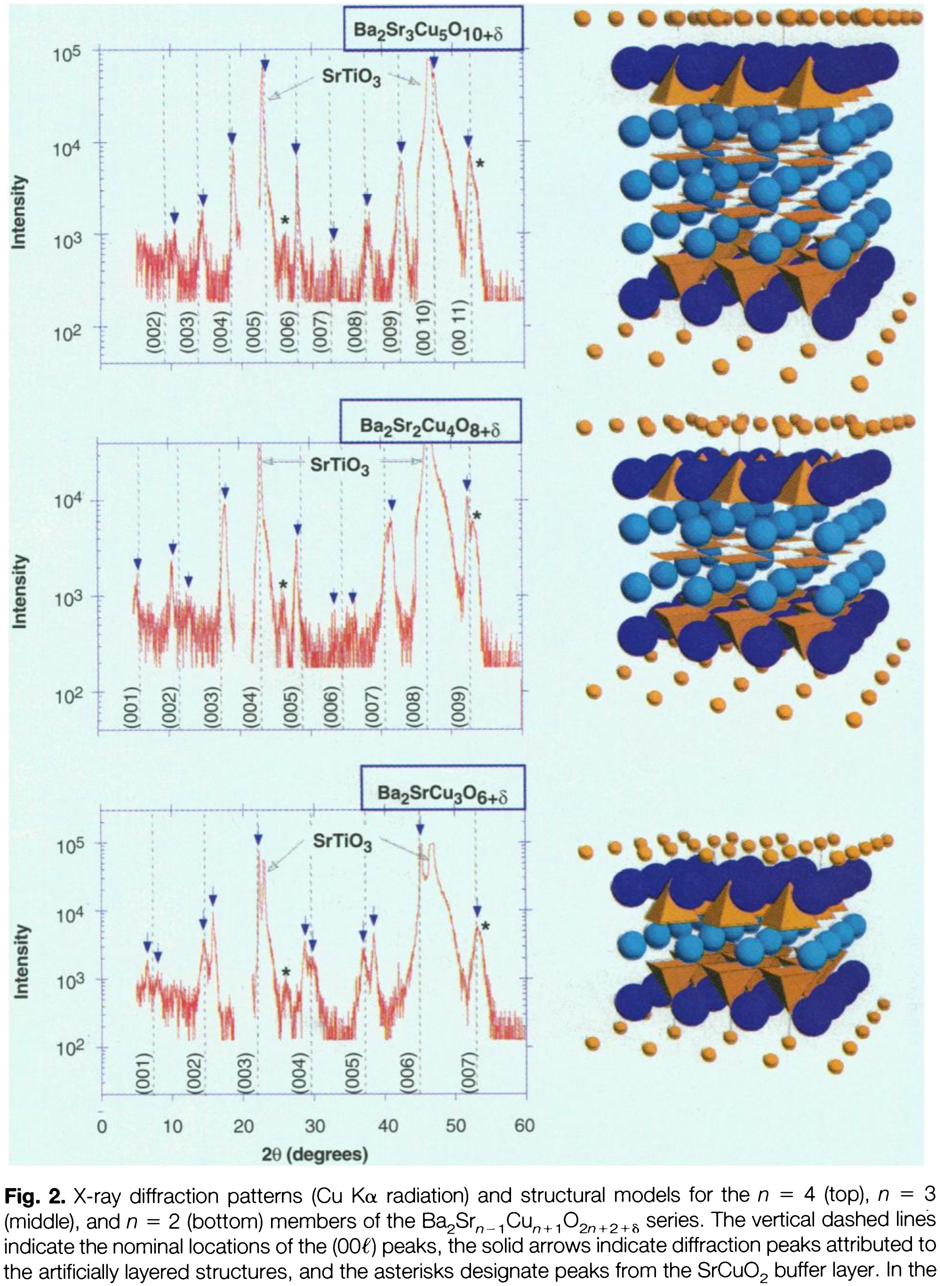

Fig. 2. X-ray diffraction patterns (Cu Kα radiation) and structural models for the $n = 4$ (top), $n = 3$ (middle), and $n = 2$ (bottom) members of the $Ba_2Sr_{n-1}Cu_{n+1}O_{2n+2+\delta}$ series. The vertical dashed lines indicate the nominal locations of the (00ℓ) peaks, the solid arrows indicate diffraction peaks attributed to the artificially layered structures, and the asterisks designate peaks from the $SrCuO_2$ buffer layer. In the models, the Ba, Sr, and Cu atoms are represented by the large, medium, and small spheres, respectively, and the CuO_4 and CuO_5 units are shown as shaded polyhedra.

cells per multilayer period. The deviations observed in the peak locations indicate that the chemical modulation is slightly incommensurate with the structural modulation for all three structures considered in Fig. 2. The fact that the peak intensities are somewhat weaker than expected indicates the presence of some Ba-Sr disorder. Because these thin films were formed as artificially layered superlattices by the sequential deposition of $SrCuO_2$ and $BaCuO_2$ layers, such disorder is expected to arise from substrate surface roughness and slight inaccuracies in the deposition rates. The x-ray diffraction patterns give *c*-axis lattice constants of the structural periodicities for the $n = 2$, 3, and 4 films of 12.1, 15.7, and 19.2 Å, respectively; the chemical periodicities for the same structures are 14.0, 17.7, and 19.9 Å, respectively. These values yield $SrCuO_2$ and $BaCuO_2$ subunit cell spacings of 3.55 and 4.28 Å, respectively, which are within 5% of the bulk value for $SrCuO_2$ and the assumed value for $BaCuO_2$ layers in the high-pressure $CuBa_2Ca_{n-1}Cu_nO_{2n+2+\delta}$ phase (*4–6*). Four-circle x-ray diffraction data show these structures to be tetragonal with in-plane lattice constants of 3.9 Å, thus matching the lattice constant for the $SrTiO_3$ substrates.

In these artificially layered structures, the $SrCuO_2$ and $BaCuO_2$ subunits could have the ideal infinite layer structure consisting of fourfold coordinated CuO_2 planes separated by oxygen-free alkaline-earth (Sr or Ba) layers, with no apical oxygen for any of the copper atoms. However, this structure seems unlikely because all of the hole-doped superconductors have apical oxygen associated with at least some of the copper atoms, and thermoelectric power measurements indicate that these materials are hole conductors (*19*). The more reasonable possibility is that the Ba planes contain some oxygen, thus creating apical oxygen and increasing the Cu coordination. The schematics of the $Ba_2Sr_{n-1}Cu_{n+1}O_{2n+2+\delta}$ structures shown in Figs. 1 and 2 assume this to be true. It is not clear, however, whether oxygen on the Ba planes resides there at the expense of oxygen on specific Cu planes. Because of this uncertainty, we have designated the materials $Ba_2Sr_{n-1}Cu_{n+1}O_{2n+2+\delta}$ and $Ba_4Sr_{n-1}Cu_{n+2}O_{2n+6+\delta}$, which makes no inference about whether inequivalent Cu sites are present, although this may occur.

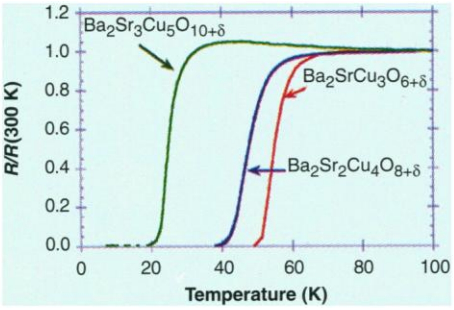

Fig. 3. Normalized resistance plotted as a function of temperature for the $n = 2$, 3, and 4 members of the $Ba_2Sr_{n-1}Cu_{n+1}O_{2n+2+\delta}$ series.

Figure 3 shows the normalized resistances for the $n = 2$, 3, and 4 members of $Ba_2Sr_{n-1}Cu_{n+1}O_{2n+2+\delta}$. The room-temperature resistivities are 1 to 5 milliohm·cm. The $n = 2$ member has the highest T_c with T_c(onset) = 70 K and $T_c(R = 0) = 50$ K. The $n = 3$ member has T_c(onset) = 60 K and $T_c(R = 0) = 40$ K, and the $n = 4$ member has T_c(onset) = 40 K and $T_c(R = 0) = 20$ K. The current density used in the measurement was ~50 A/cm². Thus far, only modest attempts have been made to optimize the superconducting properties of these materials.

In addition to $Ba_2Sr_{n-1}Cu_{n+1}O_{2n+2+\delta}$, superconductivity is also observed in the series designated $Ba_4Sr_{n-1}Cu_{n+3}O_{2n+6+\delta}$. The x-ray diffraction pattern for the $n = 3$ member of this series (Fig. 4A) indicates that the structural and chemical modulation periodicities are both ~23.75 Å. Superconductivity is observed with T_c(onset) = 70 K and $T_c(R = 0) = 40$ K (Fig. 4B). These films are stable over time if stored in a dry atmosphere.

In addition to the $n \geq 2$ members, we have attempted to synthesize the $n = 1$ member of both series, which would be $BaCuO_2$ in the infinite layer structure. If this material exists and superconducts, the small *c*-axis lattice constant (4.2 or 8.4 Å, depending on the oxygen ordering) should make it less anisotropic than other HTSc materials. Unfortunately, attempts to grow reasonably thick films of $BaCuO_2$ in the infinite layer structure have thus far been unsuccessful. However, we have stabilized $BaCuO_2$ layers ~40 Å thick in the infinite layer structure within 32 Å–40 Å $SrCuO_2$-$BaCuO_2$ multilayers. This film has a strongly metallic resistivity with a T_c(onset) near 70 K (Fig. 4B) that we attribute to the $BaCuO_2$ layer. The nonzero resistivity observed for $T < 50$ K is an artifact of the measurement caused by the electrically insulating $SrCuO_2$ cap layer (32 Å thick) that was grown to protect the $BaCuO_2$ layers from degradation. Significant positive magnetoresistance is observed for $T \leq 70$ K, which is consistent with superconductivity. We found that dc magnetometry revealed the presence of quasistatic persistent currents with a magnetization that was hysteretic in low magnetic fields. From the magnitude of the hysteresis for increasing versus decreasing field history, we estimate, on the basis of the Bean critical state model (*20*), that the circulating critical current density is $\sim 2 \times 10^4$ A/cm² at 5 K. These classical superconductive features document the fact that this multilayer structure superconducts over large areas. The magnetic signal disappeared near 36 K, somewhat below the $R = 0$ point, as a result of the stringent criterion that there be well-connected macroscopic paths for circulating currents. Thus, it appears that $BaCuO_2$, epitaxially stabilized in the infinite layer structure, superconducts. Unfortunately, we were not able to determine if oxygen ordering occurred, allowing one to differentiate between $BaCuO_2$ or $Ba_2Cu_2O_4$ (inequivalent Cu sites).

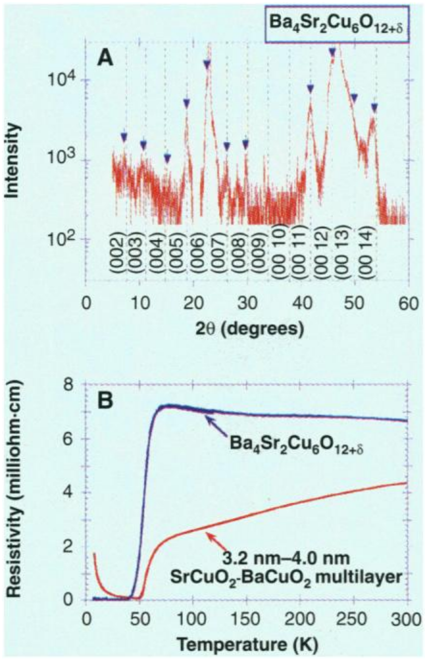

Fig. 4. The (**A**) x-ray diffraction pattern and (**B**) resistivity for the $n = 3$ member of the $Ba_4Sr_{n-1}Cu_{n+3}O_{2n+6+\delta}$ series. Also shown in (B) is the resistivity for the 3.2 nm–4.0 nm $SrCuO_2$-$BaCuO_2$ multilayer structure.

The $n = 1$ member of the $Ba_2Sr_{n-1}Cu_{n+1}O_{2n+2+\delta}$ series apparently has a value of T_c that is as high or higher than the $n > 1$ members. This behavior differs from that observed for other HTSc series, in which T_c increases as n increases. One possible explanation is that these $Ba_2Sr_{n-1}Cu_{n+1}O_{2n+2+\delta}$ films are not optimally doped, suggesting that T_c might increase with an increase or decrease in the hole carrier density. Another possibility is that the use of $SrCuO_2$ inhibits the transfer of charge from the $Ba_2Cu_2O_4$ layer into the CuO_2 layers adjacent to the Sr atoms. This latter scenario suggests that the superconducting transitions observed for all of these structures are attributable to the $Ba_2Cu_2O_4$ layers, with little or no coupling into the CuO_2 planes adjacent to the Sr atoms. This interpretation is consistent with the observed behavior for $YBa_2Cu_3O_7$-$PrBa_2$ Cu_3O_7 superlattices, where T_c decreases as the layer thickness of the nonsuperconducting $PrBa_2Cu_3O_7$ increases (*21–23*).

REFERENCES AND NOTES

1. J. G. Bednorz and K. A. Muller, *Z. Phys. B* **64**, 189 (1986).
2. T. A. Vanderah, *Chemistry of Superconductor Materials* (Noyes, Park Ridge, NJ, 1992).
3. A. Schilling *et al.*, *Nature* **363**, 56 (1993).
4. H. Ihara *et al.*, *Jpn. J. Appl. Phys.* **33**, L503 (1994).
5. C.-Q. Jin, S. Adachi, X.-J. Wu, H. Yamauchi, S. Tanaka, *Physica C* **223**, 238 (1994).
6. M. A. Alario-Franco *et al.*, *ibid.* **222**, 52 (1994).
7. Z. Hiroi *et al.*, *Nature* **364**, 315 (1993).
8. J. N. Eckstein *et al.*, *Appl. Phys. Lett.* **57**, 931 (1990).
9. T. Terashima *et al.*, *Phys. Rev. Lett.* **65**, 2684 (1990).
10. M. Y. Chern, A. Gupta, B. W. Hussey, *Appl. Phys. Lett.* **60**, 3045 (1992).
11. D. P. Norton, B. C. Chakoumakos, J. D. Budai, D. H. Lowndes, *ibid.* **62**, 1679 (1993).
12. C. Niu and C. M. Lieber, *J. Am. Chem. Soc.* **114**, 3570 (1992).
13. M. Yoshimoto, H. Nagata, J. Gong, H. Ohkubo, H. Koinuma, *Physica C* **185**, 2085 (1991).
14. M. Kanai, T. Kawai, S. Kawai, *Appl. Phys. Lett.* **58**, 771 (1991).
15. T. Siegrist *et al.*, *Nature* **334**, 231 (1988).
16. T. Kawai, Y. Egami, H. Tabata, S. Kawai, *ibid.* **349**, 200 (1991).
17. M. Lagues *et al.*, *Science* **262**, 1850 (1993).
18. X. Li, T. Kawai, S. Kawai, *Jpn. J. Appl. Phys.* **33**, L18 (1994).
19. S. D. Obertelli, J. R. Cooper, J. L. Tallon, *Phys. Rev. B* **46**, 14928 (1992).
20. W. A. Fietz and W. W. Webb, *Phys. Rev.* **178**, 657 (1969).
21. D. H. Lowndes, D. P. Norton, J. D. Budai, *Phys. Rev. Lett.* **65**, 1160 (1990).
22. J.-M. Triscone *et al.*, *ibid.* **64**, 804 (1990).
23. Q. Li *et al.*, *ibid.*, p. 3086.

24. We thank P. H. Fleming for assistance with substrate preparation. This research was sponsored by the Division of Materials Sciences, U.S. Department of Energy, under contract DE-AC05-84OR21400 with Martin Marietta Energy Systems.

9 June 1994; accepted 9 August 1994

Complete Nucleotide Sequence of *Saccharomyces cerevisiae* Chromosome VIII

M. Johnston, S. Andrews, R. Brinkman, J. Cooper, H. Ding, J. Dover, Z. Du, A. Favello, L. Fulton, S. Gattung, C. Geisel, J. Kirsten, T. Kucaba, L. Hillier, M. Jier, L. Johnston, Y. Langston, P. Latreille, E. J. Louis,* C. Macri, E. Mardis, S. Menezes, L. Mouser, M. Nhan, L. Rifkin, L. Riles, H. St. Peter, E. Trevaskis, K. Vaughan, D. Vignati, L. Wilcox, P. Wohldman, R. Waterston, R. Wilson, M. Vaudin

The complete nucleotide sequence of *Saccharomyces cerevisiae* chromosome VIII reveals that it contains 269 predicted or known genes (300 base pairs or larger). Fifty-nine of these genes (22 percent) were previously identified. Of the 210 novel genes, 65 are predicted to encode proteins that are similar to other proteins of known or predicted function. Sixteen genes appear to be relatively recently duplicated. On average, there is one gene approximately every 2 kilobases. Although the coding density and base composition across the chromosome are not uniform, no regular pattern of variation is apparent.

To identify all of the genes that constitute a simple eukaryotic cell, an international collaborative effort is under way to determine the sequence of the *Saccharomyces cerevisiae* genome. This is an important goal because of the central importance of yeast as a model organism for the study of functions basic to all eukaryotic cells. The sequences of the first two yeast chromosomes to be completed (*1*, *2*) have revealed that more than two-thirds of yeast genes have not been previously recognized and are thus novel, and the functions of more than half of these cannot be predicted, because they are not similar to proteins of known function. Here, we describe the DNA sequence of yeast chromosome VIII, which provides another 210 previously unrecognized genes and further illuminates features of yeast chromosome organization.

The sequence was determined (*3*) from the set of 23 partially overlapping phage λ and cosmid clones shown in Fig. 1 that were previously mapped by Riles *et al.* (*4*). The order of Hind III and Eco RI sites predicted from the sequence is consistent with the physical map of these sites determined independently by Riles *et al.* (*4*), which confirms that the sequence was assembled correctly. We estimate the accuracy of the sequence to be better than 99.99% (*5*). The genes and other features of the chromosome VIII sequence are listed in Table 1.

The sequence contains 269 nonoverlapping open reading frames (ORFs) greater than 300 base pairs (bp). On the basis of the analysis of Dujon *et al.* (*2*, *6*), approximately 7% of these are likely to be false genes. Thirteen of these ORFs (4.8%) are predicted to be interrupted by introns at the extreme 5′ end of each gene. The average gene size is 482 codons; the longest ORF (YHR099w) spans 11,235 bp (3745 codons).

Fifty-nine of the genes (22%) were previously identified (that is, already present in the public databases). Another 65 of the ORFs (24%) are predicted to encode proteins that are similar to genes of known or predicted function (see Table 1 for a list). Thus, the function of only 46% of the encoded proteins is known or can be predicted (in some cases, only the biological process that the protein is involved in is

Table 1. List of genes and features of chromosome VIII. The number of the cosmid (as submitted to GenBank) and its accession number are listed above the elements included in that database entry. **Column 1**: Nucleotide position of the start of each designated element (ATG for ORFs, the first nucleotide of all other elements). For the LTRs of the *Ty* elements, the beginning of the left LTR and the end of the right LTR is listed. **Column 2**: Genes are named according to established convention: Y designates yeast; H designates chromosome VIII; L and R designate the left or right chromosomal arm, respectively; w and c designate that the gene is encoded on the top or bottom strand, respectively; and a superscript "s" denotes genes predicted to be spliced. Genes are numbered from the CEN toward each TEL (telomere). Transfer RNA names also follow convention: t designates tRNA; the next letter is the one-letter code for the amino acid inserted by the tRNA (abbreviations for the amino acid residues are A, Ala; F, Phe; H, His; P, Pro; Q, Gln; S, Ser; T, Thr; and V, Val.); the letters in parentheses are the codon recognized by the tRNA; and w and c designate that the tRNA is on the top (w) or bottom (c) strand. Retrotransposon LTRs in brackets are partial elements. **Column 3**: Genetic names of genes previously identified. Note that one previously identified gene does not have a locus name (YHR042w) and that two genes (HXT5/YHR096c and ACT5/YHR129c) were named during the course of this work. **Column 4**: A description of the function of the genes. A description of the protein most similar to the other genes is also listed. Genes with no listing in this column have no homologs (BLASTX score usually less than 70). **Column 5**: The BLASTX (*18*) score for the alignment of the encoded protein to its closest homolog. Note that BLASTX scores are not listed for previously identified genes, because the two sequences are identical. BLASTX scores greater than 100 are generally considered to indicate a significant relation between two proteins; scores between 70 and 100 are considered suggestive of a relation. **Column 6**: Database accession number of the closest homolog. In the few cases where comparison of predicted proteins to the BLOCKS database (*19*) revealed potential similarities not found by BLAST, the number of the BLOCKS entry is given.

Genome Sequencing Center and Department of Genetics, Washington University School of Medicine, St. Louis, MO 63110, USA.

*Yeast Genetics, Institute of Molecular Medicine, John Radcliffe Hospital, Oxford OX3 9DU, England.